SUPPLEMENT MATERIAL

Detailed Methods

Tissue preparation

Japanese white rabbits weighing 2.4–2.9 kg were anesthetized with intravenous sodium pentobarbital (50 mg/kg). After a thoracotomy was performed, the heart was quickly excised, and the aorta was connected to a Langendorff apparatus and perfused at a pressure of 66 mmHg with Tyrode's solution (pH 7.40) containing (mmol/L): 130 NaCl, 4 KCl, 1 $MgCl_2$, 1.2 NaH_2PO_4, 1.8 $CaCl_2$, 5.6 glucose and 24 $NaHCO_3$. The perfusion solution was equilibrated with 95% O_2/5% CO_2 at 37°C.

After the heart was allowed to recover in fresh Tyrode's solution for 10 min, the right ventricular (RV) free wall was peeled off from the heart taking care to avoid damage to the coronary artery. We trimmed the RV free wall to a rectangular shape while the connection to the left ventricle (LV) remained intact (Online Figure IA). The tissue was glued to tissue supports, as shown in Online Figure IA, with a cyanoacrylate tissue adhesive (Vetbond™; 3M, St. Paul, MN). The left edge of the tissue was attached to a linear motor (ET-126A; Labworks Inc., Costa Mesa, CA) for application of linear stretches to the tissue and a displacement transducer (IW12; TWK-Elektronik, Düsseldorf, Germany) was used to measure the length of the various stretches. We set the right coronary artery in parallel with the stretch direction. The reaction force in the direction of the stretch was also measured with a force transducer (FORT-1000; World Precision Instruments, Sarasota, FL). To make the tissue taut, we applied a force of 10 gf, which defined our 0% stretch level. Zirconia beads (diameter, 0.5 mm) were attached to the myocardial surface as landmarks for motion tracking and strain measurement. At this point, the curvature of the RV surface was negligible and we assumed that the preparation was flat. To avoid tissue damage from the direct electrical stimuli, two Ag-AgCl electrodes were attached to the LV wall for ventricular pacing. The shapes of the action potentials measured on the RV surface under these conditions did not differ appreciably from those in whole heart preparations, thereby indicating that the procedures for the RV free wall preparation did not cause significant damage to the tissue and that the electrical activation was propagated from the LV normally (Online Figure II). ECG was recorded by electrodes. The measured signals were digitized at 2 kHz with a 12-bit analog-to-digital converter and stored in the hard disk of a personal computer (PC).

All experimental procedures were performed in strict accordance with the Guiding Principles for the Care and Use of Animals in the Field of Physiological Sciences approved by the Physiological Society of Japan and were approved by the National Cardiovascular Center Research Institutional Committee.

Whole heart preparation

Whole hearts from Japanese white rabbits weighing 2.4–2.9 kg were connected to a Langendorff apparatus using the same method described above. After the heart was stabilized in fresh Tyrode's solution for 10 min, a compliant polyvinyl chloride balloon was inserted into the RV. The balloon was connected to a water-filled piston pump system based on an electromagnetic shaker and a linear power amplifier (ARB-126; AR Brown, Tokyo, Japan) for rapid volume changes (Online Figure III). The volume changes were controlled by monitoring the motion of the piston with a displacement transducer (IW12; TWK-Elektronik). Volume commands were generated by a computer. Zirconia beads (diameter, 0.5 mm) were attached to the myocardial surface as landmarks. In these experiments, however, they were only used for correction of motion artifacts because the curvature of the RV surface prevented their use for strain measurement. Two Ag-AgCl electrodes were attached to the LV apex for ventricular pacing. ECG was recorded by electrodes. The measured signals were digitized at 2 kHz with a 12-bit analog-to-digital converter and stored in the hard disk of a PC.

Optical mapping of transmembrane potentials on the epicardial surface

Schematic representations of the experimental systems used are shown in Online Figure IB and Online Figure III. The methods used for recording transmembrane activity from the arterially perfused RV free walls and whole hearts were similar to those described in a previous study [1]. The tissues or hearts were loaded with a voltage-sensitive dye, di-4-ANEPPS (5 μmol/L), for 20 min. The epicardial surfaces of the tissues or hearts were illuminated by filtered excitation light (480±10 nm) obtained from bluish-green light-emitting diodes (Nichia Chemical Industries, Tokushima, Japan). The emitted fluorescent light was collected by a high numerical aperture complex photographic lens (50mm F/1.2; Nikon, Tokyo, Japan) and was split by a dichroic mirror (580nm; Andover, Salem, NH) and narrowed down to two frequency bands (540±20 nm and 680±20 nm; Andover, Salem, NH) through bandpass filters. The dual-wavelength lights were simultaneously collected by two independent complementary metal oxide semiconductor (CMOS) cameras with image intensifiers (FASTCAM-Ultima; Photron, Tokyo, Japan). The optical images were captured at a speed of 500 frames/s and a resolution of 256×256 pixels and stored in a PC. No electromechanical uncoupling agents were used.

Image processing

To account for motion artifacts caused by the stretch or contraction from the optical signals, we used ratiometry combined with a recently developed motion tracking technique [1]. For motion tracking, the initial images were chosen as a reference. In these reference images, several bead landmarks were selected manually. The corresponding positions of landmarks in the current image were automatically determined by finding the optimal local correlation of the surrounding image. We used template matching of the image of each bead with its surroundings between the resting state and the stretched state to determine the displacement of the landmark beads at high resolution (0.12 mm). These positional data were used for two purposes. First, the distances between the markers in the stretched

state were divided by the corresponding distances in the reference state to yield the epicardial local strain. Second, we used the positional data to determine the affine transformation matrices for the geometric distortion during the stretch or contraction. By using affine transformation, we mapped the sequential changes in fluorescence in the original resting geometry. Subsequently, ratiometry with numerator wavelengths of 540±20 nm and denominator wavelengths of 680±20 nm was used to remove the artifacts caused by motion along the light path. After the spatial and temporal filtering, we constructed isochronal maps of activation to determine the excitation points or the excitation propagation pattern. Moreover, phase analysis was used to study the initiation of excitations and the pattern of wave propagations [2].

Stretch protocol for tissue preparations

The protocol for applying stretch to tissue preparations is shown in Online Figure IVA. In each experiment, a stretch pulse (S2) was preceded by at least 20 electrical pulses (S1: amplitude, 2 mA; duration, 2 ms; 2 Hz) to stabilize the tissue conditions. We applied a trapezoidal command signal with a fixed plateau phase (P) at 50 ms and a rise and fall rate of 0.5% of the tissue length/ms. The amplitude was set at 5%, 10%, 15%, 20%, 25% or 30% of the tissue length and the sequence was randomized. The coupling interval (I2) between the last S1 and S2 was set at 500 ms.

Volume pulse protocol for whole heart preparations

Two types of protocols were used for whole heart preparations (Online Figure IVB). In protocol (a), after hearts were paced electrically from the RV apex 20 times, volume pulses of varying amplitudes (0.5, 1.0, 1.5 and 2.0 ml) were applied in the diastolic phase (500 ms after the electrical stimulus) to observe the stretch-induced depolarization. Because the rise and fall rate of the pulses was made constant at 0.1 ml/ms and the total duration of the pulse was also made constant (60 ms), the plateau phase (P) varied from 20~50 ms. In protocol (b), after 20 electrical stimuli from the RV apex, volume pulses of varying amplitudes (1.0, 1.5 and 2.0 ml) and constant duration (50 ms) were applied at various coupling intervals (90~130 ms). The rise and fall rate of the pulses was made constant at 0.2 ml/ms.

Pharmacological intervention

To elucidate whether the stretch-induced excitation originated from SACs, we examined the effects of Gd^{3+}. To avoid precipitation of $GdCl_3$, an oxygenated physiological salt solution (pH 7.40) was used containing (mmol/L): 137 NaCl, 5.4 KCl, 1.8 $CaCl_2$, 0.5 $MgCl_2$, 5 Hepes and 5.6 glucose. This solution was bubbled with 100% O_2 at 37°C [3, 4]. After perfusion with the salt solution in the presence of 10 μmol/L Gd^{3+} for 10 min, we recorded the optical signals in response to a 15% stretch of the ventricular tissue. We then repeated the same procedure after 15 min of perfusion with the salt solution without Gd^{3+} (washout).

We further examined the effects of ryanodine, a blocker of Ca^{2+} release channels on the sarcoplasmic

reticulum. Briefly, we applied a 15% stretch to the tissue in the presence of 200 μmol/L ryanodine.

3D structure recording system

After the measurements of both tissues and whole heart preparations, the RV wall was isolated from the heart and glued to the bottom of a saline-filled chamber via its epicardial surface with the Vetbond™ cyanoacrylate tissue adhesive. Care was taken to protect the tissue against drying by sealing the chamber with a thin polyvinylidene chloride film during the measurements. The chamber was placed on an automatic X-Y stage (KST-50XY; Sigma Koki, Tokyo, Japan) and the endocardial surface was scanned with a laser displacement meter (LK-G30; Keyence, Osaka, Japan) every 0.5 mm in both the X and Y directions to construct a wall thickness map. We discarded the thickness data for the margin because deformation caused by trimming and gluing was observed in this area.

Data analysis

To examine the inter-relationships among the isochronal map of electrical excitation, the strain distribution and the thickness distribution, each specimen was divided into 3×3 blocks of equal size and the spatially averaged data in each block were used for analyses.

To compare the optical membrane potentials among the preparations, we used the normalized value defined as follows:

$$\text{Normalized } \Delta F_{540}/F_{680} = \frac{\text{Mean } \Delta F_{540}/F_{680} \text{ of depolarization}}{\text{Peak } \Delta F_{540}/F_{680} \text{ of action potential}}$$

where $\Delta F_{540}/F_{680}$ is the ratiometric value of the optical signal. To normalize $\Delta F_{540}/F_{680}$, we used the amplitude of preceding action potential initiated by the electrical stimulus (S1).

To compare the thickness distributions among the preparations, we used the normalized thickness value of each block defined as follows:

$$\text{Normalized thickness value} = \frac{\text{Mean thickness value of each block (mm)}}{\text{Mean thickness value of all the blocks (mm)}}.$$

To compare dF/dt max (time derivative of the ratiometric optical signal) among the preparations, we used normalized values defined as follows:

$$\text{Normalized dF/dt max} = \frac{\text{Max d}(F_{540}/F_{680})/\text{dt of action potential upstroke}}{\text{Peak } \Delta F_{540}/F_{680} \text{ of action potential}}.$$

To estimate the probability of tissue excitation (y) as a function of the stretch ratio, strain or normalized thickness (x), the following logistic regression curve with a two-parameter equation was used:

$$y = \frac{1}{1+\exp(a+bx)}$$

where a and b are regression coefficients.

To evaluate the relationship between changes in the membrane potentials (y) (under threshold) and local strain (x), we used the following non-linear regression curve with a two-parameter equation:

$$y = a\left(1 - \exp(-bx)\right)$$

where a and b are regression coefficients.

The conduction velocity (CV) was calculated as the distance traveled normal to isochrones of activation per unit time. The CVs in the unstretched state and stretched state are defined as follows [5]:

$$CV_{unstretched} = \frac{L_0}{\Delta t(L_0)}$$

$$CV_{stretched} = \frac{L_0}{\Delta t(L_1)}$$

where $\Delta t(X)$ is the conduction time measured over the two-point distance X. L_0 and L_1 are the unstretched and stretched two-point distances, respectively.

The relationships between the thickness and the strain and between the normalized dF/dt max and the local strain were assessed by univariate linear regression analysis and the Pearson correlation coefficient test. A repeated-measures ANOVA was used to evaluate the drug effects. When there was a significant difference, Tukey's test was applied for multiple comparisons. In the whole heart preparations, difference in the excitation probability among four groups of normalized thickness was analyzed by one-way ANOVA followed by Bonferroni's test. Data were expressed as means ± SEM. Values of $P<0.05$ were considered statistically significant.

Supplemental References

1. Inagaki M, Hidaka I, Aiba T, Tatewaki T, Sunagawa K, Sugimachi M. High resolution optical mapping of cardiac action potentials in freely beating rabbit hearts. *Conf Proc IEEE Eng Med Biol Soc.* 2004;5:3578-3580.
2. Gray RA, Pertsov AM, Jalife J. Spatial and temporal organization during cardiac fibrillation. *Nature.* 1998;392:75-78.
3. Caldwell RA, Clemo HF, Baumgarten CM. Using gadolinium to identify stretch-activated channels: technical considerations. *Am J Physiol.* 1998;275:C619-621.
4. Kiseleva I, Kamkin A, Wagner KD, Theres H, Ladhoff A, Scholz H, Gunther J, Lab MJ. Mechanoelectric feedback after left ventricular infarction in rats. *Cardiovasc Res.* 2000;45:370-378.
5. Mills RW, Narayan SM, McCulloch AD. The Effects of Wall Stretch on Ventricular Conduction and Refractoriness in the Whole Heart. In: Kohl P, Sachs F, Franz MR, eds. *Cardiac Mechanoe-Electric Feedback and Arrhythmias: From Pipette to Patient.* Philadelphia: Elsevier Sauders; 2005:127-136.

Supplemental Figure Legends

Online Figure I. Tissue preparation and the experimental setup.

A: A photograph of the tissue preparation. Scale bar: 5 mm.

B: Schematic representation of the experimental setup. The excised RV wall with its intact coronary artery is glued to a pair of tissue supports connected to a force transducer (FT) and a linear motor (LM). ECG, force (f) and displacement (d) signals are amplified (Amp) and recorded by an AD converter (A/D) and personal computer (PC). Stretch and electrical stimulation commands are generated by the PC and applied to the LM and an electrical stimulator (Stim) through a DA converter (D/A). For optical mapping, the tissue is illuminated by light emission diodes (LED). The fluorescent emission light is split by a dichroic mirror (DM) and narrowed down to two frequency bands by appropriate filters (F1 and F2). Optical images are captured by two independent CMOS cameras (CMOS) with image intensifiers (I.I) and stored in a memory controller (M/C) and the PC. L: lens.

Online Figure II. Action potential shapes of tissues and whole heart preparations.

Upper figure: Representative optical signals initiated by an electrical stimulus are shown for a tissue (left) and a whole heart preparation (right). Lower figure: 50% repolarizations of the action potential duration (APD50) are shown for a tissue and a whole heart preparation. Scale bar: 100 ms. NS: no significance.

Online Figure III. Experimental setup for the whole heart study.

A: Schematic representation of the experimental setup. A balloon (B) is inserted into the RV of the perfused whole heart. The balloon is connected to a piston pump (P) with a linear motor (LM). ECG and volume (V) signals are amplified (Amp) and recorded by an AD converter (A/D) and a personal computer (PC). Stretch and electrical stimulation commands are generated by the PC and applied to the LM and an electrical stimulator (Stim) through a DA converter (D/A). For optical mapping, the heart is illuminated by light emission diodes (LED). The fluorescent emission light is split by a dichroic mirror (DM) and narrowed down to two frequency bands by appropriate filters (F1 and F2). Optical images are captured by two independent CMOS cameras (CMOS) with image intensifiers (I.I) and stored in a memory controller (M/C) and the PC. L: lens.

Online Figure IV. Stretch and volume pulse protocols.

In both tissue and whole heart studies, a stretch/volume pulse (S2) is preceded by a train of pulses (S1: 2 Hz) to stabilize the heart conditions. In the tissue study (A), the coupling interval between the last S1 and S2 (I2) is set at 500 ms. The plateau (P) and velocity (V) of the stretch are 50 ms and 0.5%/ms, respectively. The amplitude of the stretch (E) is set at 5%, 10%, 15%, 20%, 25% or 30% of the tissue length. In the whole heart study (B), two different protocols were applied (a and b). In protocol (a), the coupling interval between the last S1 and S2 (I2) was set at 500 ms and the entire

duration (T) and the speed (V) of the volume pulses were set at 60 ms and 0.1 ml/ms, respectively. The amplitude of the volume pulses (E) was set at 0.5, 1.0, 1.5 or 2.0 ml. In protocol (b), I2 was varied from 90 to 130 ms. The entire duration (T) and the speed (V) of the volume pulses were set at 50 ms and 0.2 ml/ms, respectively. The amplitude of the volume pulses (E) was set at 1.0, 1.5 or 2.0 ml.

Online Figure V. Excitation and its modulation by shorter stretches.

A: Representative isochronal maps of optical mapping data in response to 10% and 25% stretches with a shorter entire time duration (50 ms). Scale bar: 4 mm. **B:** Ratiometric optical signals in response to 10% and 15% stretches with various timings (phases 2, 3 and 4) during the cardiac cycle. The transient stretch applied in phase 2 elicited a repolarization. The transient stretch applied in late phase 3 or phase 4 elicited a depolarization which was sometimes followed by a premature ventricular contraction. Scale bar: 50 ms.

Online Figure VI. Stretch-induced excitation from the center and conduction velocity.

A: Left panel: Representative isochronal maps of a membrane potential showing the focal excitation from the center region initiated by a 15% stretch. Right panel: Corresponding thickness distributions. Scale bar: 2 mm. **B:** a, Comparison of the vertical CVs between the excitations initiated by an electrical stimulus (electric stim) and a 10% stretch. b, Comparison of the horizontal CVs between the excitations initiated by an electrical stimulus and a 10% stretch. Left panels: Representative isochronal maps for the electrical stimuli. Right panels: Representative isochronal maps for the 10% stretches. Scale bar: 4 mm.

Online Figure VII. Relationship between dF/dt maximums and local strains.

Relationships between the normalized dF/dt max (maximum value of the time derivative of the ratiometric optical signal) of the action potential upstrokes and local strains in response to 10% (open circle), 20% (closed black rectangle) and 30% (closed gray square) stretches. Line is a linear regression line ($n=5$, $r=-0.40$, $P<0.0001$).

Online Figure VIII. Phase dependency of the stretch-induced excitations

The excitation probabilities in response to volume pulses of 1.0 ml (closed triangles) or 1.5 ml (closed squares) with various coupling intervals (90, 100, 110, 120, 130, 150, 200 and 500 ms) were evaluated.

Supplemental Figures

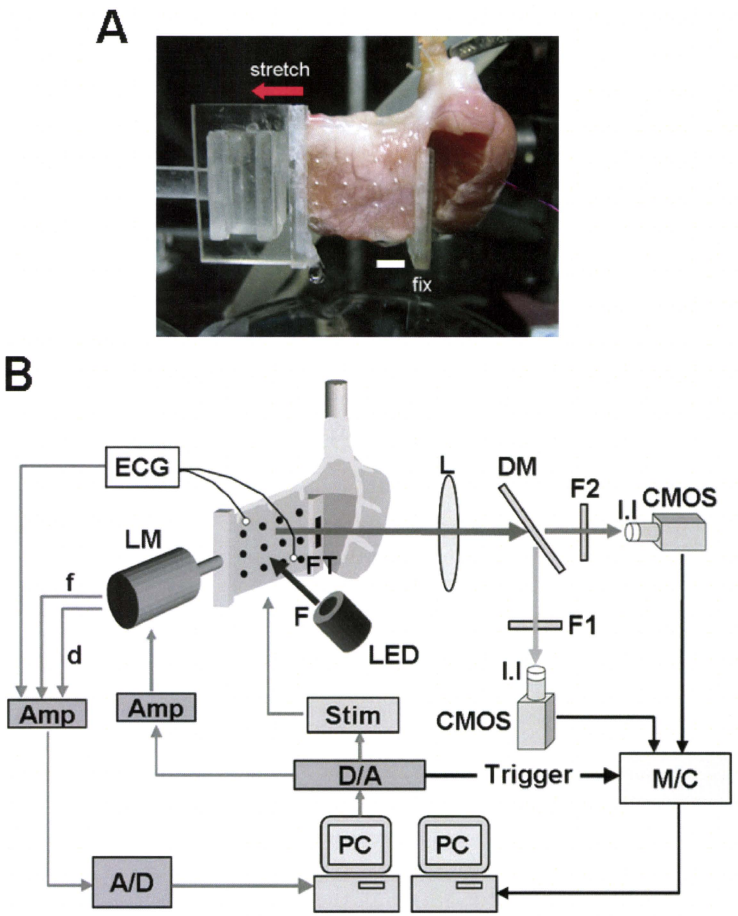

Online Figure I

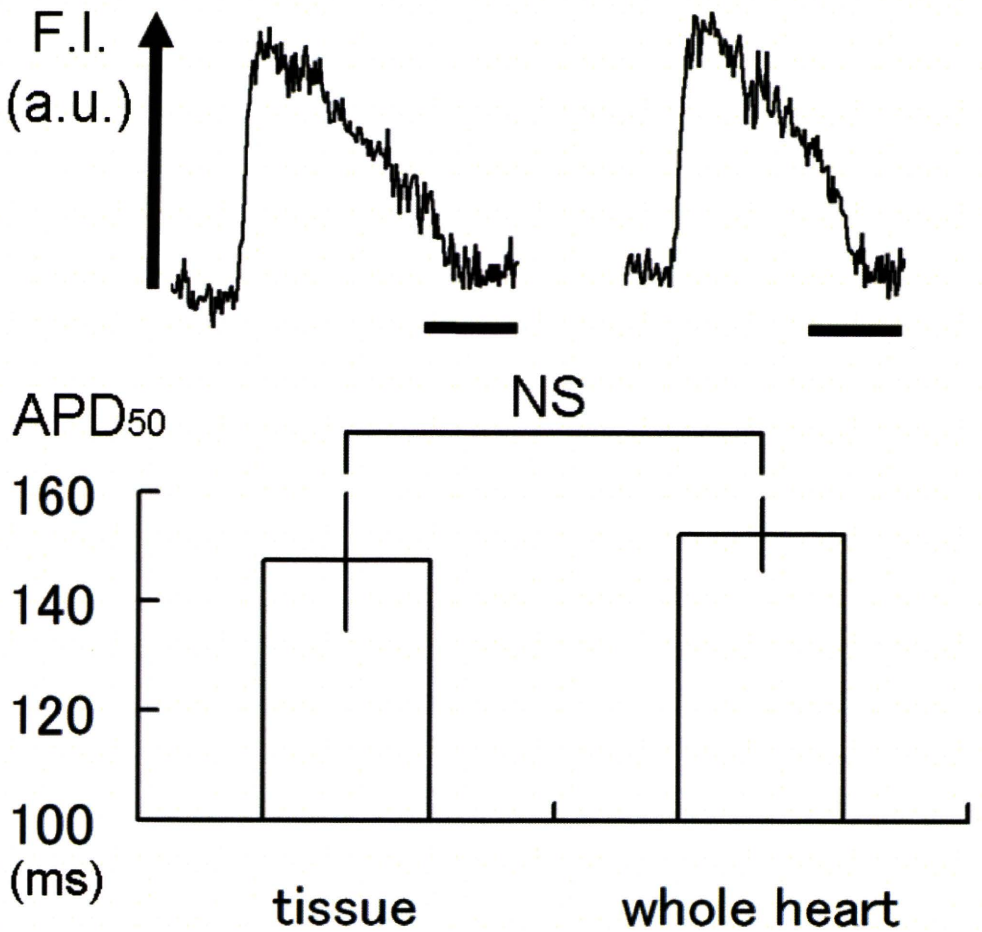

Online Figure II

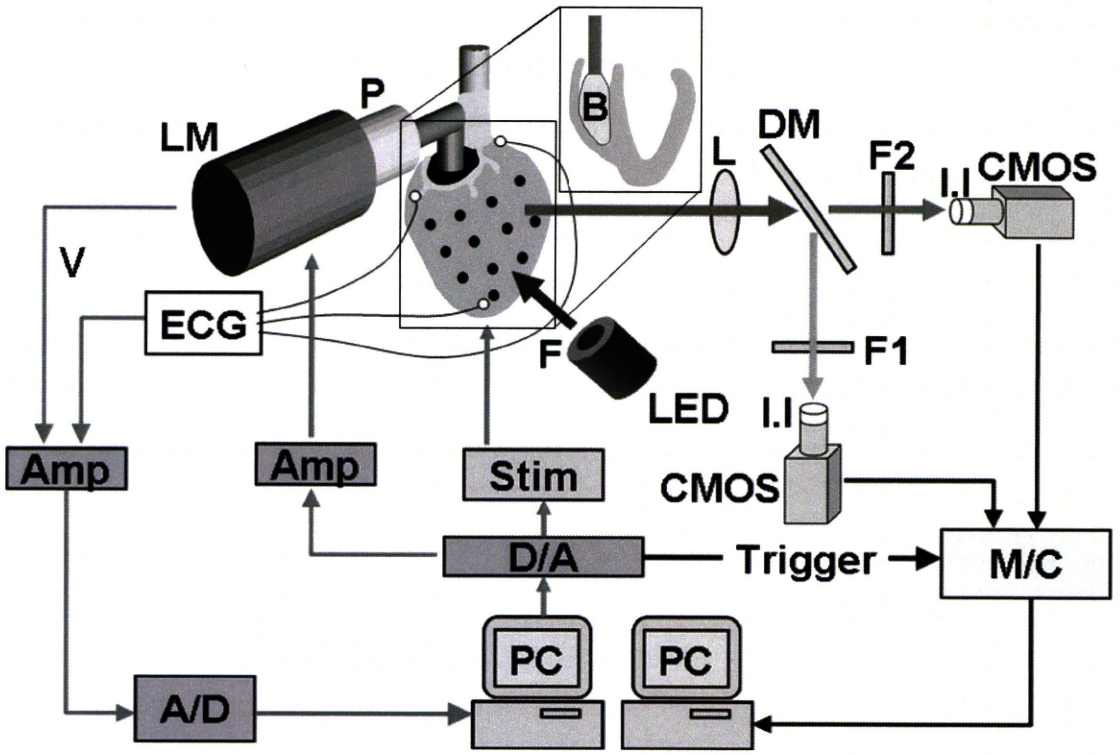

Online Figure III

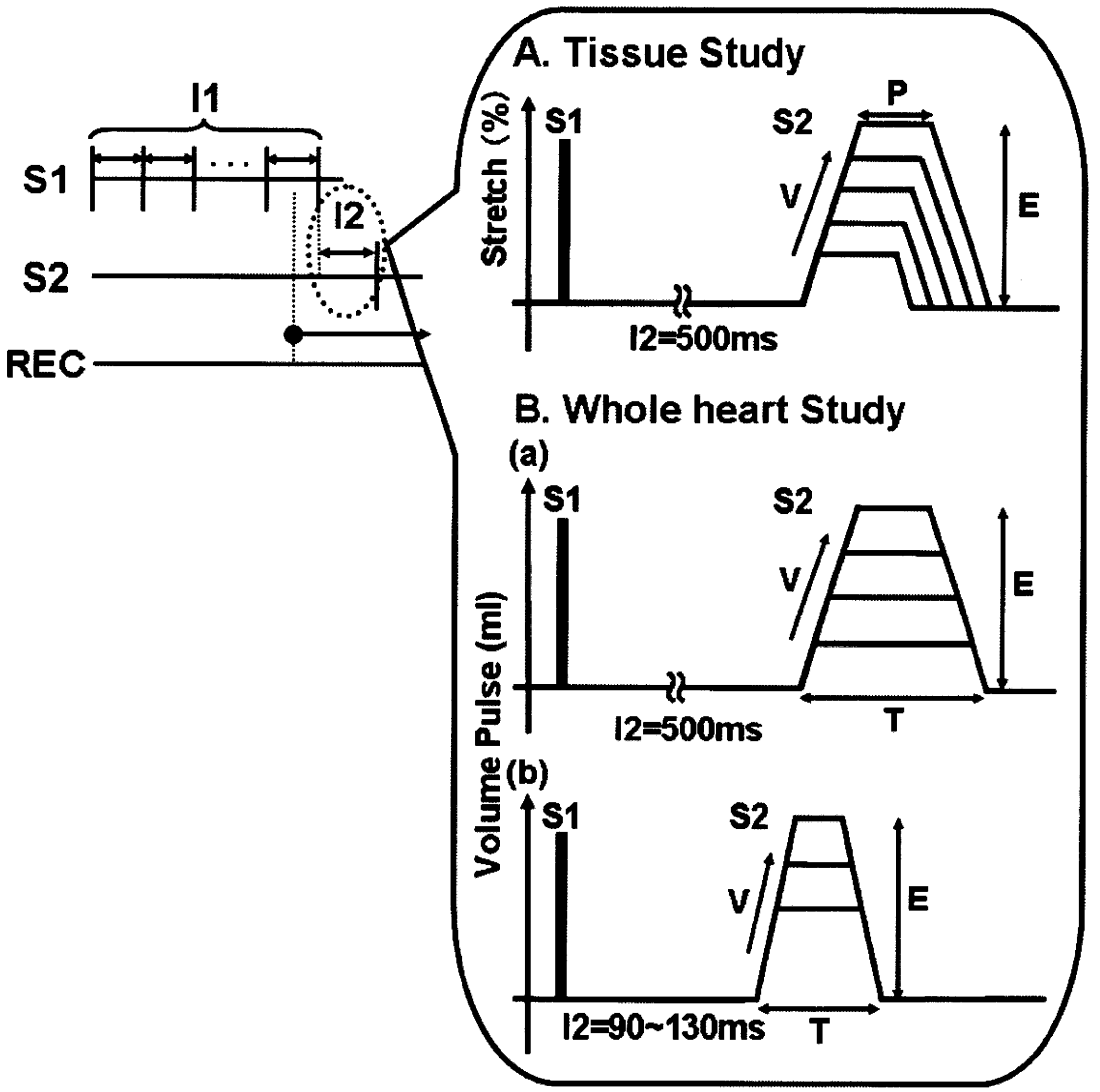

Online Figure IV

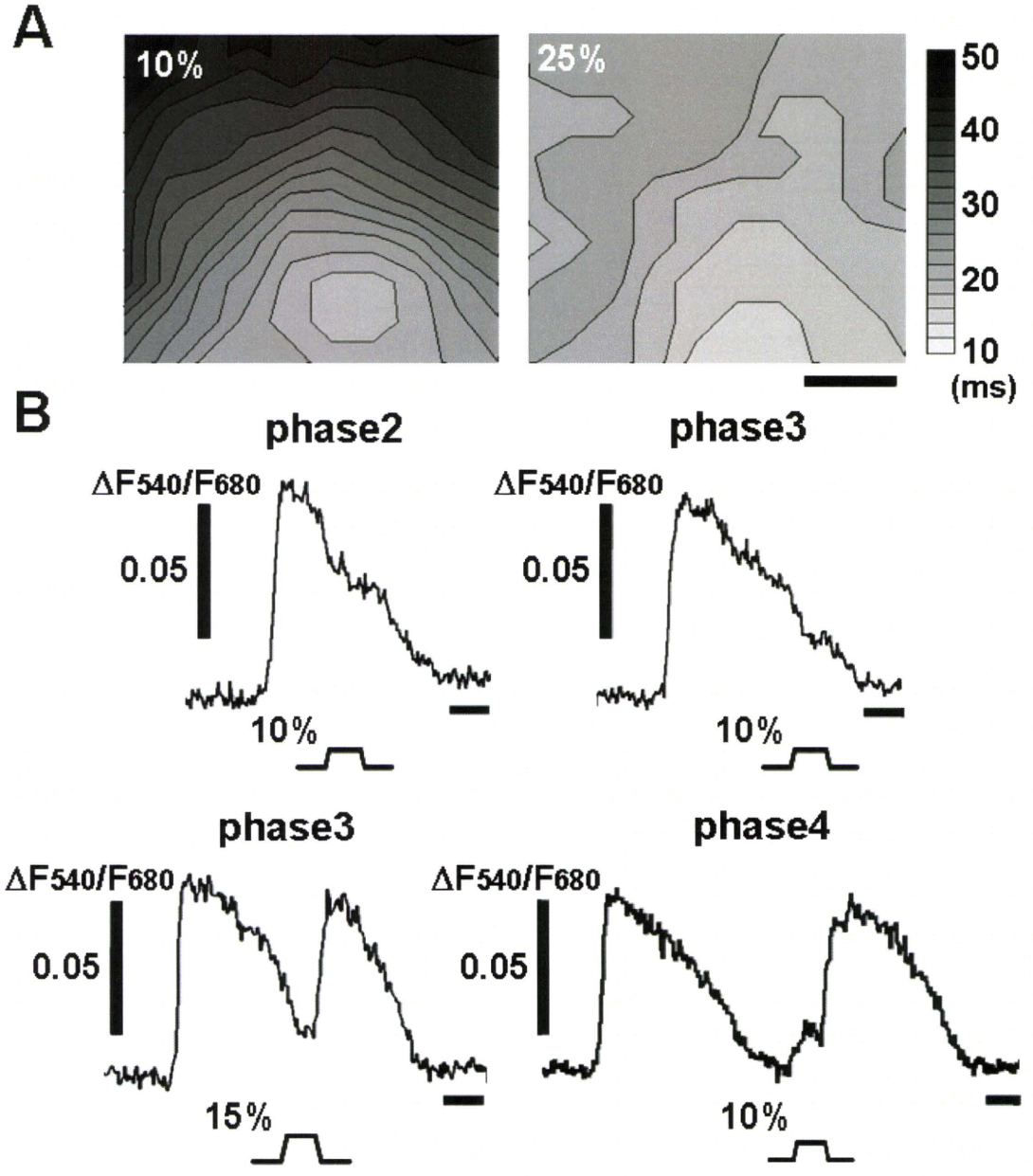

Online Figure V

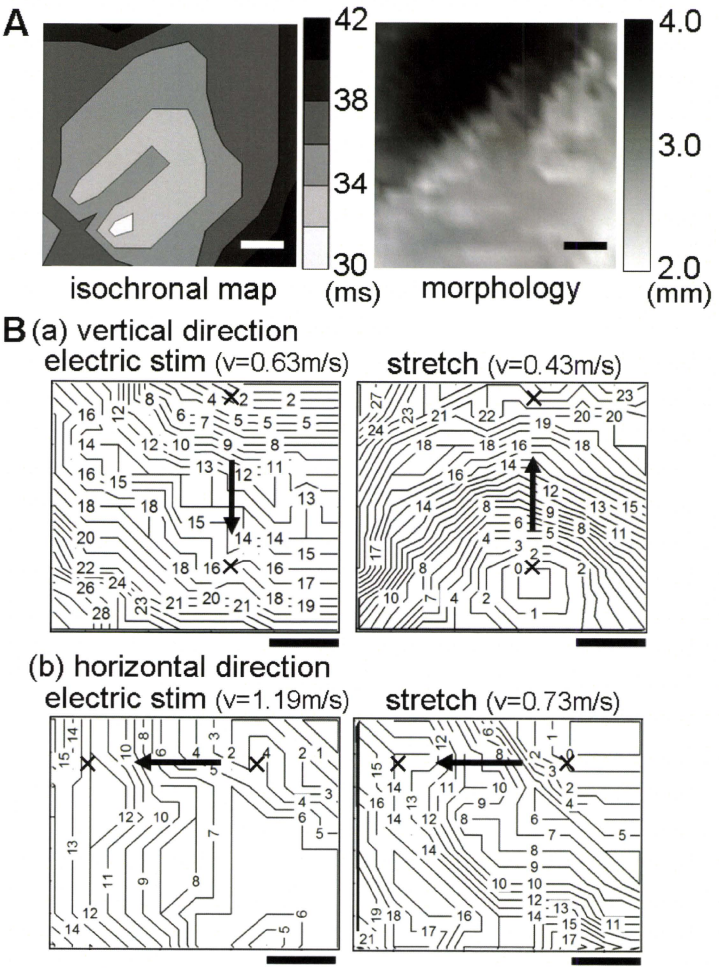

Online Figure VI

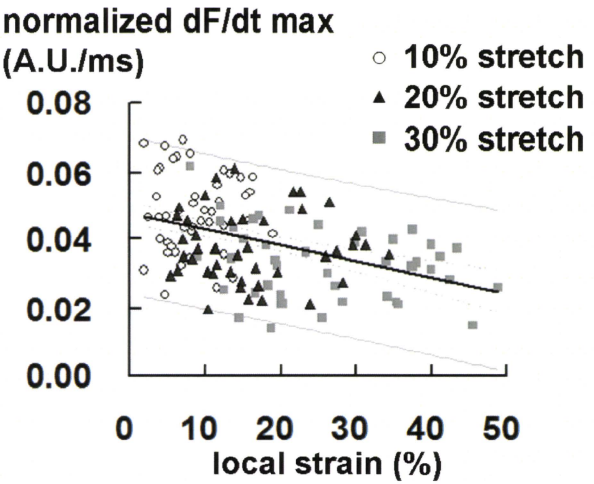

Online Figure VII

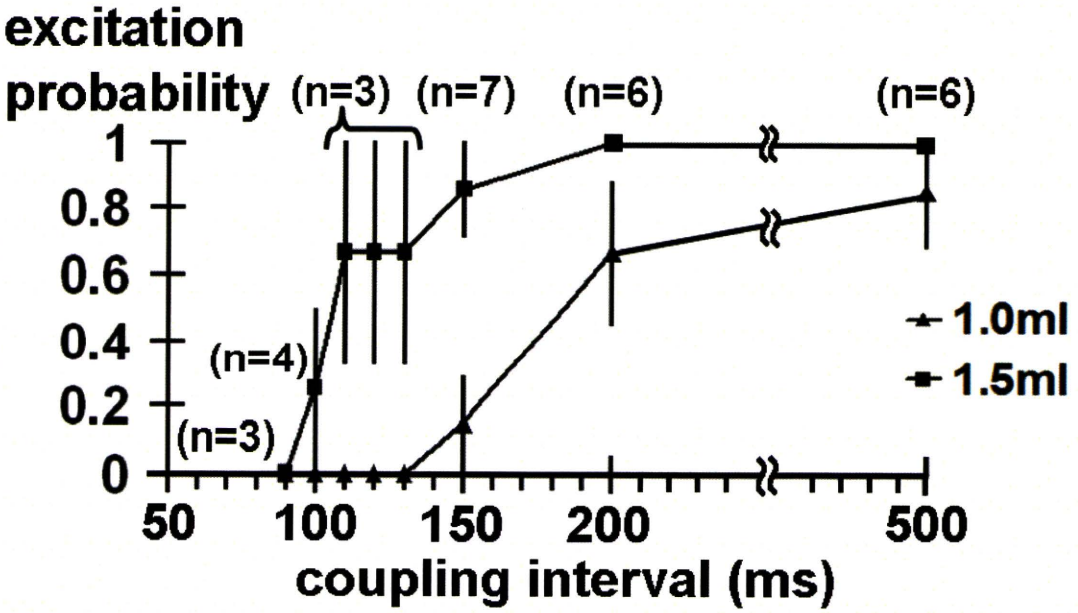

Online Figure VIII

Comput Mech (2010) 46:247–258
DOI 10.1007/s00466-009-0432-1

ORIGINAL PAPER

Study of efficient homogenization algorithms for nonlinear problems

Approximation of a homogenized tangent stiffness to reduce computational cost

Jun-ichi Okada · Takumi Washio · Toshiaki Hisada

Received: 30 January 2009 / Accepted: 10 October 2009 / Published online: 31 October 2009

Abstract A framework for the homogenization of nonlinear problems is discussed with respect to block LU factorization of the micro–macro coupled equation, and based on the relation between the characteristic deformation and the Schur-Complement as the homogenized tangent stiffness. In addition, a couple of approximation methods are introduced to reduce the computational cost, i.e., a simple scheme to reuse the old characteristic deformation and a sophisticated method based on the mode-superposition method developed by our group. Note that these approximation methods satisfy the equilibrium conditions in both scales. Then, using a simplified FE model, the conventional algorithm, a relative algorithm originating from the block LU factorization, and the above-mentioned algorithms with the approximated Schur-Complement are compared and discussed. Finally, a large-scale heart simulation using parallel computation is presented, based on the proposed method.

Keywords Homogenization method · Nonlinear finite element analysis · Schur-Complement · Mode superposition · Parallel computation · Block LU factorization · Heart

List of symbols

$\mathbf{Y}, \mathbf{y}$	Position vector around the deformation in the microstructure
$\mathbf{X}, \mathbf{x}$	Position vector around the deformation in the macrostructure
$\mathbf{u}$	Macroscopic displacement vector
$\{\mathbf{u}\}$	Macroscopic structure nodal displacement vector
$\{\mathbf{u}^e\}$	Macroscopic structure nodal displacement vector per element
$\mathbf{w}$	Periodic component of the microscopic displacement vector
$\{\mathbf{w}\}$	Periodic component of the nodal displacement vectors of all microstructures
$\{\mathbf{w}^Q\}$	Periodic component of the nodal displacement vector of a single microstructure
$\{\mathbf{w}^e\}$	Periodic component of the nodal displacement vector per element
$\mathbf{F}$	The deformation gradient tensor
$\mathbf{Z}$	The displacement gradient tensor
$\mathbf{C}$	The right Cauchy–Green tensor
$\mathbf{E}$	The Green–Lagrange strain tensor
Π	The first Piola–Kirchhoff stress tensor
$\mathbf{I}$	The identity tensor
I_c, II_c, III_c	Principal invariants
J	Determinant $\mathbf{F}$

J. Okada (✉) · T. Washio · T. Hisada
Graduate School of Frontier Sciences, University of Tokyo,
5-1-5 Kashiwanoha, Kashiwa, Chiba 277-8563, Japan
e-mail: okada@sml.k.u-tokyo.ac.jp

1 Introduction

The door to petaflop computing has recently opened and meaningful applications for massively parallel computers are being sought. A multi-scale approach to biomechanical problems is consequential in the post-genome era and the homogenization method is going to play a more important role than ever before. The homogenization method is a mathematical modeling technique for efficiently analyzing inhomogeneous material with a periodic microstructure. In

biomaterial, the periodicity hypothesized in the homogenization method is not strictly established. However, Terada et al. [1] have shown that an appropriate equivalent characteristic is obtained in material with an irregular microstructure by assuming a periodic boundary condition. Thus, it is possible to evaluate the effect of each component in the microstructure on the macroscopic behavior, if microstructure modeling is appropriate. The homogenization method for biomaterial was applied to bone by Hollister and Kikuchi [2], while a two-dimensional analysis of engineered tissue cells was conducted by Breuls et al. [3]. In an example using the heart, Krassowska et al. [4] applied the method to an excitation propagation phenomena. To investigate the effect of intracellular structure on heartbeat, the authors have developed the necessary finite element homogenization method, where the heart is the macrostructure and the cardiomyocyte the microstructure. Thus the problem inevitably becomes a large-scale one.

In the homogenization method two scales are introduced, namely, a scale for the unit period, and a scale for the whole material. By solving the governing equations for both scales with coupling, we can obtain the macroscopic characteristic as an equivalent homogeneous body and variable distribution from the microstructure. In the conventional nonlinear homogenization method [5,6], it is first necessary to calculate microscopic equilibrium and then the macroscopic tangential homogenization updates all quadrature points at every Newton–Raphson iteration, resulting in huge computational cost. Even with a high performance computer, the cost is prohibitive for practical large-scale problems. To reduce this computational cost, various techniques have been devised. These include, for example, the construction of a database with the homogenized properties [7], sensitivity analysis [8], Fast Fourier Transforms [9], and so on. In a previous work, we proposed a homogenization method using characteristic deformation mode superposition [10,11]. This is, however, an approximation method and the accuracy depends on the problem. We subsequently proposed a new algorithm that solves the microscopic equilibrium equation alternately with the solution of the mode superposition-based micro–macro coupled equation. In this algorithm, the equilibrium conditions for both the micro and macro structures are satisfied with far less computational cost. This method is applicable to microstructures composed of slightly incompressible and viscoelastic materials [12–15].

Looking at this method from the block LU factorization of the micro–macro coupled equation, we recognize that the Schur-Complement as the homogenized tangent stiffness, is ingeniously approximated with the aid of mode superposition. It is further beneficial to generalize this view, that is, to interpret the framework of the homogenization method with regard to the block LU factorization and investigate how the Schur-Complement can be approximated to reduce the computational cost whilst preserving the accuracy. Accordingly, a couple of approximation methods, i.e., a simple scheme to reuse the old characteristic deformation and the above-mentioned mode-superposition based method, are introduced in this paper. Then a simplified numerical example is solved using both the conventional homogenization algorithm and the algorithm originating from the block LU factorization, and the performance of each is discussed. Finally, a large-scale heart simulation using parallel computation is presented based on the proposed method.

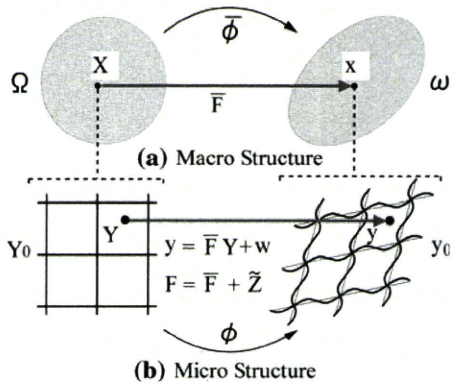

Fig. 1 Homogenization method for large deformation problems. **a** Macro structure. **b** Micro structure

2 Homogenization method for finite deformation problem

2.1 Problem statement and geometric prospect

We assume that the material in the body (Ω) reveals heterogeneity on a very fine scale and is characterized by the periodic distribution of a basic structural element (Y_0) as shown in Fig. 1. To measure the changes in the spatial domains, we introduce two scales: a macro-scale $X \in \Omega$ and a micro-scale $Y \in Y_0$. Thus the actual domain can be regarded as the product space ($\Omega \times Y_0$). In the subsequent development, the macroscopic quantity corresponding to the microscopic one is expressed with a bar symbol over the microscopic symbol. The following assumptions of homogenization are applied in the formulation of the homogenization method.

- A macrostructure that consists of a periodic microstructure can be considered to be an approximately equivalent homogeneous substance.
- A microstructure is infinitely fine compared with a macrostructure; the variable defined at each point of the macrostructure corresponds to the volume average of the variables in the microstructure.

It is assumed that the deformation of the microstructure is linked to the local values of the macro continuum via

$$\mathbf{y} = \overline{\mathbf{F}}\mathbf{Y} + \mathbf{w}, \tag{1}$$

where $\mathbf{y}$ and $\mathbf{Y}$ are position vectors defined on the microstructure [16].

The deformation consists of a homogeneous part $\overline{\mathbf{F}}\mathbf{Y}$ and a non-homogeneous superposed field $\mathbf{w}$. Consequently, the following relationships exist between the microscopic and macroscopic deformation gradients.

$$\mathbf{F} = \nabla_Y \mathbf{y} = \frac{\partial \mathbf{y}}{\partial \mathbf{Y}} = \overline{\mathbf{F}} + \tilde{\mathbf{Z}}, \tag{2}$$

$$\overline{\mathbf{F}} = \nabla_X \mathbf{x} = \frac{\partial \mathbf{x}}{\partial \mathbf{X}}, \tag{3}$$

$$\tilde{\mathbf{Z}} = \nabla_Y \mathbf{w} = \frac{\partial \mathbf{w}}{\partial \mathbf{Y}}. \tag{4}$$

Thus increment and variation of the deformation gradients are represented, respectively, as

$$\Delta\mathbf{F} = \Delta\overline{\mathbf{F}} + \Delta\tilde{\mathbf{Z}} = \Delta\overline{\mathbf{F}} + \nabla_Y \Delta\mathbf{w}, \tag{5}$$

$$\delta\mathbf{F} = \delta\overline{\mathbf{F}} + \delta\tilde{\mathbf{Z}} = \delta\overline{\mathbf{F}} + \nabla_Y \delta\mathbf{w}. \tag{6}$$

For the assumptions mentioned above, the macroscopic gradients are related via the volume averages

$$\overline{\mathbf{F}} = \frac{1}{|V|}\int_{Y_0} \mathbf{F} dY = \frac{1}{|V|}\int_{Y_0} (\overline{\mathbf{F}} + \tilde{\mathbf{Z}}) dY = \overline{\mathbf{F}} + \frac{1}{|V|}\int_{Y_0} \tilde{\mathbf{Z}} dY, \tag{7}$$

where V is the volume of the microstructure Y_0. Then, the fluctuation field $\mathbf{w}$ must satisfy the constraint

$$\int_{Y_0} \tilde{\mathbf{Z}} dY = \int_{Y_0} \frac{\partial \mathbf{w}}{\partial \mathbf{Y}} dY = \int_{\partial Y_0} \mathbf{N} \otimes \mathbf{w} dS = \mathbf{0}, \tag{8}$$

where $\mathbf{N}$ is an outward normal vector on the boundary ∂Y_0. This constraint is satisfied when $\mathbf{w}$ is periodic.

2.2 Formulation of homogenization method and finite element discretization

We now consider the equilibrium of material with a periodic microstructure, modeled by hyperelastic material. Using the principle of stationary potential energy, the equilibrium condition becomes a functional stationary problem. Under the homogenization assumptions, the macroscopic potential energy is related via the volume averages of the microscopic ones and the entire potential energy is defined by

$$\Phi = \int_\Omega \frac{1}{|V|}\int_{Y_0} W dY dX - \int_{\partial\Omega} \mathbf{t} \cdot \mathbf{u} dS, \tag{9}$$

where W is the strain energy function of the microstructure defined by the deformation gradient $\mathbf{F}$, and assuming conservative tractions. The stationary condition becomes

$$\delta\Phi = \int_\Omega \frac{1}{|V|}\int_{Y_0} \delta\mathbf{F} : \Pi dY dX - F_{ext}(\delta\mathbf{u}) = 0, \tag{10}$$

$$\Pi = \frac{\partial W}{\partial \mathbf{F}}, \tag{11}$$

$$F_{ext}(\delta\mathbf{u}) = \int_{\partial\Omega} \mathbf{t} \cdot \delta\mathbf{u} dS. \tag{12}$$

A similar equation has been reported by Terada and Kikuchi [5] using two-scale convergence theory [17]. We have also shown a formulation based on the mixed variational principle with a perturbed Lagrange-multiplier [14]. By inserting Eq. (6) into Eq. (10), macro and micro equilibrium equations can be derived based on the defined space of the variation.

$$\overline{G} = \int_\Omega \frac{1}{|V|}\int_{Y_0} \delta\overline{\mathbf{F}} : \Pi dY dX - F_{ext}(\delta\mathbf{u}) = 0, \tag{13}$$

$$G = \int_{Y_0} \delta\tilde{\mathbf{Z}} : \Pi dY = 0, \tag{14}$$

which achieves equilibrium under the given boundary condition in the macrostructure and self-equilibrium under a periodic boundary condition, Eq. (8), of the microscopic displacement in the microstructure. Thus the homogenization method simultaneously satisfies the two equilibrium conditions as described above. To solve the nonlinear equation, the Newton–Raphson method is employed. Then the standard linearization process in nonlinear finite element method provides the following linearized equations

$$\int_\Omega \frac{1}{|V|}\int_{Y_0} \delta\mathbf{F} : \mathbf{A} : \Delta\mathbf{F} dY dX = F_{ext}(\delta\mathbf{u}) - \int_\Omega \frac{1}{|V|}\int_{Y_0} \delta\mathbf{F} : \Pi dY dX, \tag{15}$$

$$\mathbf{A} = \frac{\partial \Pi}{\partial \mathbf{F}}. \tag{16}$$

Substituting Eqs. (5) and (6) into the above equation yields

$$\int_\Omega \frac{1}{|V|}\int_{Y_0} s(\delta\overline{\mathbf{F}} + \delta\tilde{\mathbf{Z}}) : \mathbf{A} : (\Delta\overline{\mathbf{F}} + \Delta\tilde{\mathbf{Z}}) dY dX = F_{ext}(\delta\mathbf{u}) - \int_\Omega \frac{1}{|V|}\int_{Y_0} (\delta\overline{\mathbf{F}} + \delta\tilde{\mathbf{Z}}) : \Pi dY dX. \tag{17}$$

By finite element discretization using

$$\Delta\overline{\mathbf{F}} = [\overline{B^e}]\{\Delta\mathbf{u}^e\}, \tag{18}$$

$$\Delta\tilde{\mathbf{Z}} = [B^e]\{\Delta\mathbf{w}^e\}, \tag{19}$$

where $[B^e]$ is a shape function matrix, the left-hand side of Eq. (17) becomes

$$\begin{aligned}
&\{\delta \mathbf{w}^Q\}\frac{1}{|V|}\int_{Y_0}[B^e]^T[A][B^e]dY\{\Delta \mathbf{w}^Q\}\\
&\quad+\{\delta \mathbf{w}^Q\}\frac{1}{|V|}\int_{Y_0}[B^e]^T[A]dY[\overline{B^e}]\{\Delta \mathbf{u}^e\}\\
&\quad+\{\delta \mathbf{u}^e\}[\overline{B^e}]^T\frac{1}{|V|}\int_{Y_0}[A][B^e]dY\{\Delta \mathbf{w}^Q\}\\
&\quad+\{\delta \mathbf{u}^e\}[\overline{B^e}]^T\frac{1}{|V|}\int_{Y_0}[A]dY[\overline{B^e}]\{\Delta \mathbf{u}^e\}\\
&=\{\delta \mathbf{w}^Q\}\mathbf{K}^Q_{ww}\{\Delta \mathbf{w}^Q\}+\{\delta \mathbf{w}^Q\}\mathbf{K}^Q_{wu}\{\Delta \mathbf{u}^e\}\\
&\quad+\{\delta \mathbf{u}^e\}\mathbf{K}^Q_{uw}\{\Delta \mathbf{w}^Q\}+\{\delta \mathbf{u}^e\}\mathbf{K}^Q_{uu}\{\Delta \mathbf{u}^e\},
\end{aligned}\tag{20}$$

while the second term of the right-hand side of Eq. (17) becomes

$$-\{\delta \mathbf{u}^e\}[\overline{B^e}]^T\frac{1}{|V|}\int_{Y_0}[\Pi]dY-\{\delta \mathbf{w}^Q\}\frac{1}{|V|}\int_{Y_0}[B^e]^T[\Pi]dY,\tag{21}$$

at each quadrature point of the macrostructure. Symbol Q denotes the quantity that is evaluated at a macroscopic quadrature point, while symbol e denotes the quantity evaluated in the macroscopic element. By assembling these appropriately on the macro continuum, and considering the facultative variations, the following semi-positive definite symmetric matrix is obtained

$$\begin{bmatrix}\mathbf{K}_{ww} & \mathbf{K}_{wu}\\ \mathbf{K}_{uw} & \mathbf{K}_{uu}\end{bmatrix}\begin{Bmatrix}\Delta \mathbf{w}\\ \Delta \mathbf{u}\end{Bmatrix}=\begin{Bmatrix}\mathbf{r}_w\\ \mathbf{r}_u\end{Bmatrix},\tag{22}$$

where

$$\mathbf{K}_{ww}=\int_\Omega\left(\frac{1}{|V|}\int_{Y_0}[B^e]^T[A][B^e]dY\right)dX\tag{23}$$

$$\mathbf{K}_{wu}=\int_\Omega\left(\frac{1}{|V|}\int_{Y_0}[B^e]^T[A]dY\right)[\overline{B^e}]dX\tag{24}$$

$$\mathbf{K}_{uw}=\int_\Omega[\overline{B^e}]^T\left(\frac{1}{|V|}\int_{Y_0}[A][B^e]dY\right)dX\tag{25}$$

$$\mathbf{K}_{uu}=\int_\Omega[\overline{B^e}]^T\left(\frac{1}{|V|}\int_{Y_0}[A]dY\right)[\overline{B^e}]dX\tag{26}$$

$$\{\mathbf{r}_w\}=-\int_\Omega\left(\frac{1}{|V|}\int_{Y_0}[B^e]^T[\Pi]dY\right)dX\tag{27}$$

$$\{\mathbf{r}_u\}=F_{ext}-\int_\Omega[\overline{B^e}]^T\left(\frac{1}{|V|}\int_{Y_0}[\Pi]dY\right)dX.\tag{28}$$

The nonlinear homogenization method solves Eq. (22) for $\Delta\mathbf{u}$ and $\Delta\mathbf{w}$ under the given boundary condition for the macrostructure and the periodic boundary condition (Eq. 8) for microscopic displacement. The number of degrees of freedom (NDOF) of this matrix is (NDOF of macrostructure + quadrature point of macrostructure × NDOF of microstructure). An enormous computational cost is, however, required to solve a small-scale problem. Moreover, it is difficult to solve the form given in Eq. (8) due to memory limitations, and generally, a transformation into the weak form takes place as described below.

2.3 Characteristic deformation

In a nonlinear problem, to evaluate the response of a microstructure to macroscopic deformation in a similar way to that in a linear problem [18], we obtain the following equation by taking the derivative of Eq. (14) at each quadrature point and substituting Eqs. (5) and (16).

$$\int_{Y_0}\delta\tilde{\mathbf{Z}}:\mathbf{A}:d\tilde{\mathbf{Z}}dY=-\int_{Y_0}\delta\tilde{\mathbf{Z}}:\mathbf{A}:d\overline{\mathbf{F}}dY\tag{29}$$

Since the macroscopic deformation gradient is independent of the microscopic integration,

$$\int_{Y_0}\delta\tilde{\mathbf{Z}}:\mathbf{A}:\frac{\partial\tilde{\mathbf{Z}}}{\partial\overline{\mathbf{F}}}dY=-\int_{Y_0}\delta\tilde{\mathbf{Z}}:\mathbf{A}:\mathbf{I}dY,\tag{30}$$

where $\mathbf{I}$ is a fourth order identity tensor, and the microstructural response of the macroscopic deformation gradient becomes

$$\frac{\partial\tilde{\mathbf{Z}}}{\partial\overline{\mathbf{F}}}=\nabla_Y\left(\frac{\partial\mathbf{w}}{\partial\overline{\mathbf{F}}}\right)\equiv-\nabla_Y\chi,\tag{31}$$

$$\chi\equiv-\frac{\partial\mathbf{w}}{\partial\overline{\mathbf{F}}},\tag{32}$$

where a third order tensor χ is the derivative of the microscopic displacement with respect to the macroscopic deformation gradient. This is referred to as the characteristic deformation for nonlinear problems. The equation above can be substituted into Eq. (30) yielding

$$\int_{Y_0}\delta\tilde{\mathbf{Z}}:\mathbf{A}:\nabla_Y\chi dY=\int_{Y_0}\delta\tilde{\mathbf{Z}}:\mathbf{A}:\mathbf{I}dY.\tag{33}$$